3

CALCULATING SLOW-MOTION ESR SPECTRA OF SPIN-LABELED POLYMERS

KEITH A. EARLE

University at Albany, State University of New York, Albany, New York

DAVID E. BUDIL

Northeastern University, Boston, Massachusetts

Contents

Advanced ESR Methods in Polymer Research, edited by Shulamith Schlick.

1. INTRODUCTION

Electron spin resonance (ESR) spectroscopy has been widely used to obtain information about the molecular dynamics of polymers. The method requires the introduction of a stable free-radical reporter group, such as a nitroxide, into the system. Nitroxide spin labels can be covalently attached to the polymer of interest, and can therefore serve as probes of the local backbone dynamics of the polymer, providing information on the local orientation, structure, dynamics, and environment.[1–3] A commonly used nitroxide is shown in Fig. 1. Depending on the ESR frequency, motion on time scales between 10^{-3} and 10^{-10} s may be investigated by this method, making it ideal to study the dynamics of macromolecules and macromolecular structures or assemblies.

The ESR spectrum of a nitroxide is sensitive to reorientational processes because of the inherent orientation dependence (anisotropy) of the magnetic interactions of the unpaired electron with the applied magnetic field, and with the magnetic nuclei on the label. The ESR spectrum is most sensitive when these interactions are modulated by rotation on a time scale τ_c that is comparable to the inverse of the frequency width, $\Delta\omega$, of the spectrum. When $\tau_c\Delta\omega \approx 1$, the motion is said to fall within the "slow-motional" regime for the given ESR frequency. At extremely short correlation times, the spectrum approaches the fast motion limit and one observes only the isotropic average of the magnetic interactions. At very long correlation times, a static distribution of all the possible probe orientations, the "rigid limit" spectrum, is observed.

Two major approaches have been employed to calculate the ESR spectrum of a paramagnetic species that is reorienting on the slow-motional time scale. One approach is the trajectory method,[4,5] which utilizes the time-dependent trajectories of axes that are fixed in the nitroxide frame to calculate the ESR spectrum directly. The trajectories may be generated either by simulating them using single-particle Brownian dynamics,[4] or by obtaining them directly from a molecular dynamics simulation.[5,6] An alternative approach is the stochastic Liouville equation (SLE),[7,8] which can be regarded as a generalized semiclassical master diffusion equation. In this description, the electronic and nuclear spins are treated quantum mechanically,

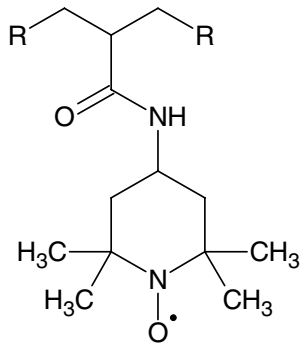

Fig. 1. A nitroxide that is commonly used in polymer spin labeling based on the commercially available 4-amino-2,2,6,6-tetramethyl piperidine-1-oxyl (TEMPAMINE) radical.

while the reorientational motion is treated classically, and parameterized in terms of rotational diffusion constants.

Of these two approaches, the SLE method enjoys much wider application to the analysis of spin-label spectra; while trajectory-based calculations remain time consuming, solution of the SLE has been rendered extremely efficient by the application of advanced sparse matrix algorithms.[9–11] On modern personal computers, a typical ESR spectrum at the conventional frequency of 9 GHz can be calculated by the SLE method in a fraction of a second. This efficiency is the major feature that enables the application of iterative analysis of the experimental line shape, as described below. Another important advantage of the SLE method is its versatility: it can be used to calculate spectra over the entire motional range of the probe, from the fast-motion limit to the rigid limit.

This chapter presents a detailed description of the analysis of slow-motional ESR spectra of spin-labeled polymers, using the SLE-based ESR line shape calculation developed by the Freed group at Cornell (EPRLL, as originally named by Schneider and Freed[10,11]). We will only present such details of the calculation as may be needed to understand how it may be most efficiently applied to ESR line shape analysis. Detailed expositions of the theory underlying the SLE equation and its implementation may be found elsewhere.[9,12–15]

We will start by surveying the parameters that are used to describe the magnetic interactions within the nitroxide label, as well as the parameters used to characterize its motion. Because of the significant number of parameters that may be required to describe the rotational dynamics, the best means of extracting information about probe structure, orientation, and dynamics is to fit a calculated ESR spectrum to the experimental one by least-squares minimization of the model parameters. The chapter describes some of the least-squares methods that have been successfully applied to this type of analysis and concludes with some illustrative examples. Specific applications to spin-labeled polymers and interpretation of the ESR parameters obtained by this analysis are described in greater detail in Chapter 6.

2. PHYSICAL PARAMETERS OF NITROXIDE LABELS

2.1. Magnetic Tensors of the Nitroxide

Analysis of a slow-motional ESR spectrum to obtain dynamic parameters requires prior knowledge of the magnetic interactions of the paramagnetic species (i.e., the parameters of the spin Hamiltonian). The two most important magnetic interactions of interest in nitroxide spin labels include (*1*) the hyperfine interaction between the electron and the nitroxide nitrogen, which may be either the ^{14}N ($I = 1$) or ^{15}N ($I = \frac{1}{2}$) nucleus; and (*2*) the g-factor anisotropy of the unpaired electron. Additional hyperfine interactions involving the ^{1}H nuclei on the nitroxide ring and vicinal methyl groups, which are typically not resolved in standard continuous wave (CW) ESR experiments, are therefore less important for obtaining dynamic information about the probe. However, these secondary hyperfine interactions give

rise to an inhomogeneous line width that should be taken into account in the analysis of the spectra.

All orientation-dependent magnetic terms in the nitroxide may be represented as "tensors" (although not all of them are true tensors in the mathematical sense). These include the nitrogen hyperfine tensor, **A**, and the electronic *g*-tensor, **g**. Each tensor is represented in terms of three principal values and a set of three associated axis directions relative to the frame of the nitroxide. First, the axis orientations are discussed.

Theoretical[16] and experimental single-crystal studies[17] have shown that the axis directions of **g** (also called the *magnetic* axes x_m, y_m, and z_m) are oriented relative to the nitroxide frame as illustrated in Fig. 2. These axes are chosen so that the corresponding principal *g*-values obey the relation $g_x > g_y > g_z$. Thus, the z_m axis lies along the axis of the p_z orbital of the nitrogen, the x_m axis is perpendicular to z_m and lies approximately along the N–O bond direction, and the y_m axis is perpendicular to these.

The principal axis directions of the **A** tensor (x_A, y_A, z_A) are specified using the Euler angles that give their orientation relative to x_m, y_m, and z_m according to the standard convention.[18] These angles are referred to as the "magnetic tilt" angles, $\Omega_m = (\alpha_m, \beta_m, \gamma_m)$. Explicitly, they specify the following set of rotations, which are also illustrated in Fig. 3: (*1*) rotation about z_m by the angle α_m, (*2*) rotation about the new *y* axis by the angle β_m, and (*3*) rotation about the new *z* axis by the angle γ_m. This is equivalent to the following set of rotations in the original reference frame: (*1*) rotation about z_m by the angle γ_m, (*2*) rotation about y_m by the angle β_m, and (*3*) rotation about z_m by the angle α_m. In this convention, positive rotation angles specify a rotation that would advance a right-handed screw along the rotation axis.

In practice, the magnetic tilt angles are almost always taken to be zero (i.e., the **A** axes are assumed to coincide with the **g** axes); however, for nitroxides in

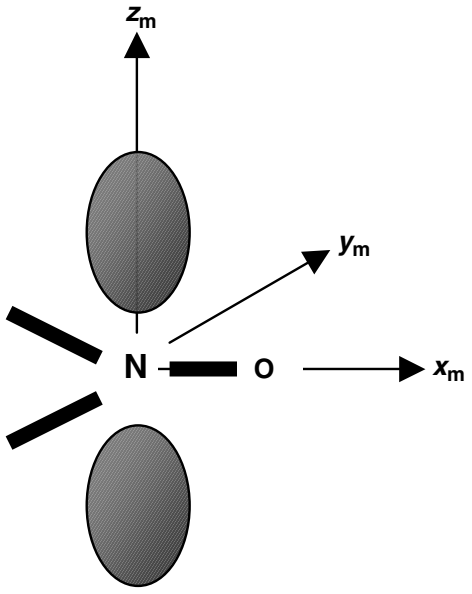

Fig. 2. Directions of the principal *g* (or magnetic) axes x_m, y_m, and z_m are oriented relative to the nitroxide molecular frame.

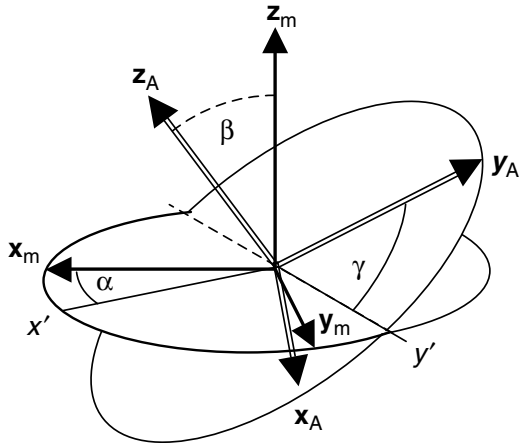

Fig. 3. Definition of the "magnetic tilt" angles, $\Omega_m = (\alpha_m, \beta_m, \gamma_m)$ that define the directions of the principal axes of the ^{14}N hyperfine tensor relative to the magnetic axes.

six-membered rings, single-crystal studies have revealed a small rotation in the *x*–*y* plane (represented by either α_m or γ_m) corresponding to "twisted boat" configurations of the ring.[17] Although such conformations are observed in single crystals, and interconversion between ring conformations should in principle contribute to the ESR line shape, conformational dynamics of the ring is typically neglected in line shape analysis of spin-labeled macromolecules.

In addition to **A** and **g**, the inhomogeneous line width tensor **W** may be specified. Here **W** is an ad hoc representation of orientation-dependent line broadening that arises from variations in the local electrostatic environment of the nitroxide. Inhomogeneous broadening of this type becomes particularly significant at higher ESR frequencies, where small variations in the **g** tensor are resolved. Moreover, this type of broadening is effectively anisotropic, since it increases in degree as the *g*-value gets further from the free-electron *g*-value. Thus, electrostatic inhomogeneity preferentially affects the g_x value of a nitroxide. The principal values of **W** represent the derivative peak-to-peak width of a Lorentzian line. Because **W** is generally used to represent *g*-factor inhomogeneity, the principal axes of **W** are taken to be the same as those of **g**.

The principal values of **g**, **A**, and **W** are most typically obtained from the rigid limit spectrum of the nitroxide. At high ESR frequencies (94 GHz and above), the features corresponding to the *x*, *y*, and *z* orientations of the nitroxide are well enough resolved that the principal values of **g** and **A** may be read directly from the spectrum, as illustrated in Fig. 4*a*. Specifically, at high field one may observe three groups of three features; the central feature of each group may be used to calculate the *g*-factor for the given orientation, and the spacing between the features gives the hyperfine interaction for that orientation. Although commercial instruments are available at frequencies up to 140 GHz, the most commonly used ESR frequency is 9 GHz. At this frequency, the features identifying the principal **g** and **A** values overlap significantly (cf. Fig. 4*b*), and it is often necessary to carry out a least-squares fitting to the experimental rigid limit line shape. Least-squares analysis is also the preferred method to determine the principal values of **W**.

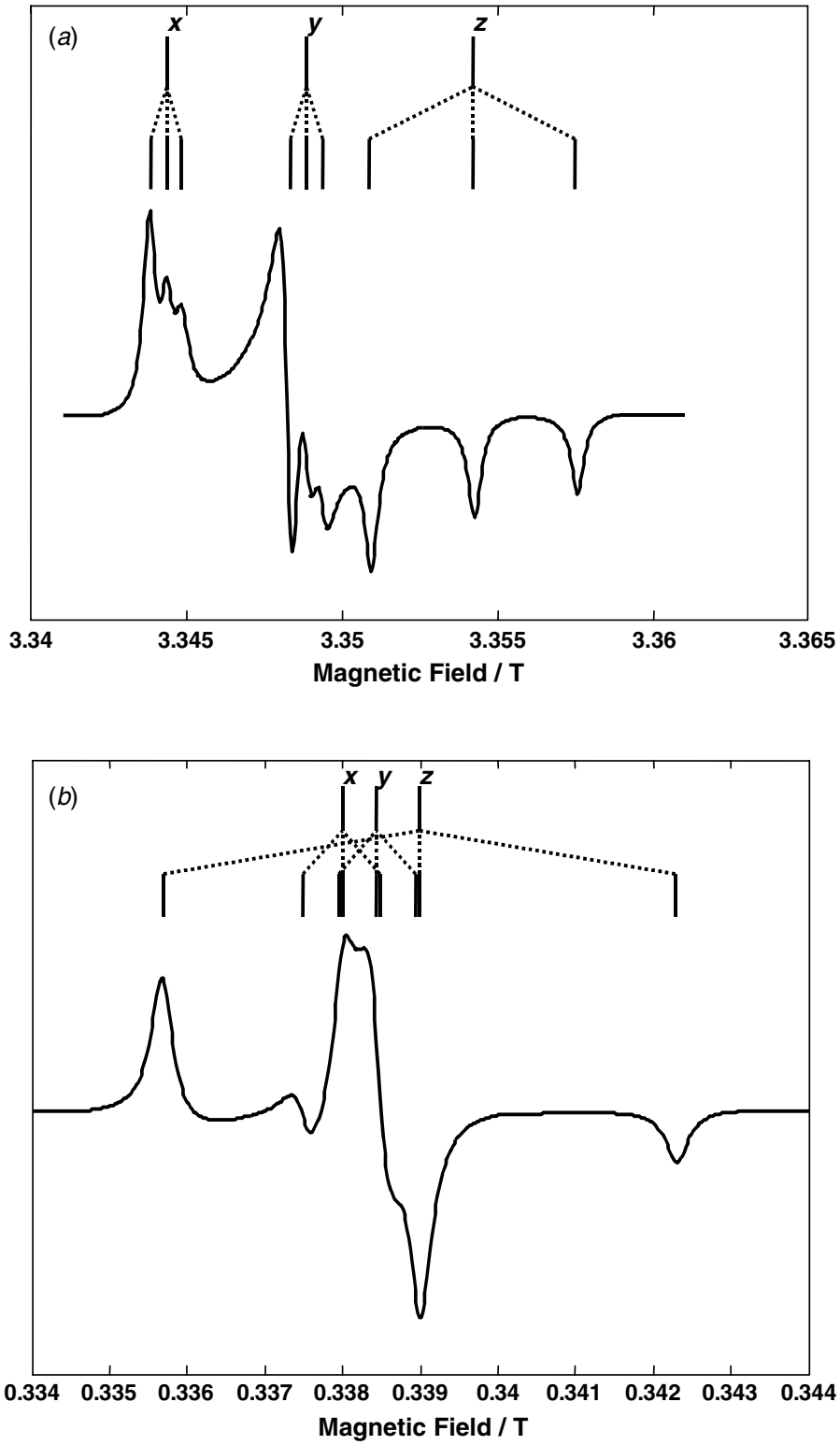

Fig. 4. Rigid limit spectra of a nitroxide at (*a*) 94 GHz and (*b*) 9 GHz. Lines indicate the location of "turning points" in the spectrum from which magnetic tensor parameters may be determined. The central lines of each group of three indicate the field positions from which the anisotropic g_x-, g_y-, and g_z- values are determined, and the spacing between the lines indicates the corresponding ^{14}N hyperfine splittings. Note the high degree of overlap in the 9-GHz spectrum.

In addition to the inhomogeneous line width tensor **W**, the EPRLL programs provide a way to account for inhomogeneous broadening that specifically arises from unresolved hyperfine interactions between the unpaired electron spin and surrounding nuclei (generally ^{1}H). This type of broadening is generally well approximated by a Gaussian line shape, and is specified as the derivative peak-to-peak width of a Gaussian line ($\Delta^{(0)}$). In liquid solution, the underlying hyperfine interactions may be treated as being isotropic; in oriented systems, such as liquid crystalline polymers or membranes, the broadening is orientation-dependent due to small anisotropies in the hyperfine interactions. Thus, the EPRLL programs provide a second Gaussian line width parameter $\Delta^{(2)}$ that accounts for the dependence of line width on the orientation angle Ψ of the membrane or liquid-crystal director (see Section 2.3) according to the definition $\Delta = \Delta^{(0)} + \Delta^{(2)}\sin^2\Psi$. It is important to note that this orientation dependence is defined relative to the director frame (defined below) and not to the magnetic axis system.

An alternative form for specifying tensor principal values that is sometimes used in the EPRLL-family programs is the "spherical" representation. In terms of the Cartesian components of a tensor **M**, namely, M_x, M_y, and M_z, its "spherical" components are defined as

$$\begin{aligned} M_1 &= (M_x + M_y + M_z)/3 \\ M_2 &= M_z - (M_x + M_y)/2 \\ M_3 &= M_x - M_y \end{aligned} \tag{1}$$

The components M_1, M_2, and M_3 are referred to as the isotropic, axial, and rhombic components of the tensor **M**, and they differ by constant factors from the respective conventional spherical tensor components, $M^{(0,0)}$, $M^{(2,0)}$, and $M^{(2,2)}$. The definition given here allows the components to be correlated directly with and/or estimated from the features of an experimental spectrum. This is illustrated in Fig. 5,

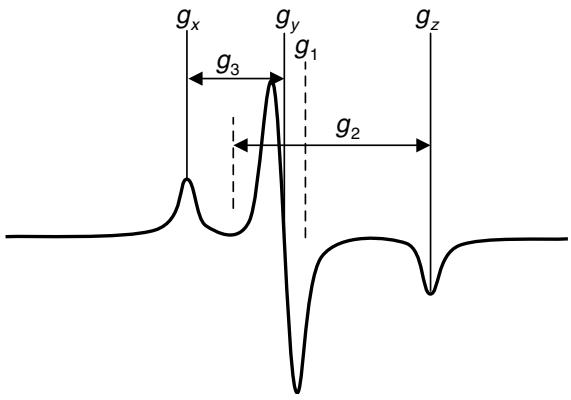

Fig. 5. Relationship between the pseudo-spherical tensor components and the turning points in the spectrum of a radical with *g* anisotropy but no nuclear hyperfine interactions. Note that the tensor components may be estimated directly from the features of the spectrum.

TABLE 1. Magnetic Parameters in the EPRLL Programs [a]

Symbol	Name	Description
g_x, g_y, g_z g_1, g_2, g_3	**gx, gy, gz** **g1, g2, g3**	Principal values of the electronic **g** matrix: Cartesian *x*, *y*, and *z* components (unitless)
A_x, A_y, A_z A_1, A_2, A_3	**ax, ay, az** **a1, a2, a3**	Principal values of the nuclear hyperfine tensor: Cartesian *x*, *y*, and *z* components (in gauss)
I	**in2**	Two times the total nuclear magnetic spin *I*.
α_m, β_m, γ_m	**alpham, betam, gammam**	Euler angles α_M, β_M, γ_M specifying the tilt of the principal axes of the nuclear hyperfine interaction relative to those of the electronic Zeeman interaction (in degrees)
γ_n	**gamman**	Nuclear gyromagnetic ratio γ_N (in
$\Delta^{(0)}$, $\Delta^{(2)}$	**gib0, gib2**	Isotropic ($\Delta^{(0)}$) and orientation-dependent ($\Delta^{(2)}$) Gaussian inhomogeneous broadening $\Delta = \Delta^{(0)} + \Delta^{(2)}\sin^2\psi$ (Gaussian derivative peak-to-peak width in Gauss)
W_x, W_y, W_z W_1, W_2, W_3	**wx, wy, wz** **w1, w2, w3**	Principal values of the orientation-dependent inhomogeneous line-broadening tensor, Cartesian *x*, *y*, and *z* components (Lorentzian derivative peak-to-peak width in gauss)

[a] (One-nucleus, one-electron spin $\frac{1}{2}$ system).

which for clarity shows the spectrum of an unpaired electron with *g* anisotropy, but without any resolved hyperfine splittings.

The spherical representation is included because it allows one to vary the tensor components in such a way that it remains axially symmetric, or maintains a constant trace. Such constraints can often be assumed based on other considerations (e.g., average hyperfine coupling from fast-motional spectra) before the least-squares fitting is undertaken. Thus, to maintain a constant isotropic value one should fix M_1 and vary M_2 and M_3; to maintain axial symmetry, M_3 should be set to zero, and M_1 and M_2 varied.

Table 1 summarizes the magnetic parameter names that are used in the EPRLL family programs to specify the spin Hamiltonian for a electron spin $S = \frac{1}{2}$ radical with a single significant nucleus, such as a nitroxide spin label.

2.2. Diffusion Models

This section summarizes some of the models for molecular motion that are implemented in currently available SLE programs for ESR line shape calculations. In the following description, parameters specifying rates or rate constants in units of reciprocal seconds (s^{-1}) will be expressed on a base 10 logarithmic scale. Thus, for example, a diffusional rate constant of 3.0×10^7 s^{-1} would be represented by the parameter

value 7.48. The major reason for this convention is that most dynamic processes of the polymer or spin label are activated processes and therefore exhibit an approximately exponential dependence upon the temperature. A second advantage is that dynamic parameters expressed on this scale are of the same order of magnitude as the other quantities used as input to the SLE, which avoids some numerical problems that may arise in least-squares minimization when the search parameters are of significantly different magnitudes.

Before discussing the different parameters used in the diffusion operator SLE formalism, it is necessary to define a number of different coordinate systems, depicted in Fig. 6*a* and *b*. The first frame of interest is the *director frame* ($\mathbf{x}_D$, $\mathbf{y}_D$, $\mathbf{z}_D$), which is fixed relative to the structure of the polymer to which the label is attached. The $\mathbf{z}_D$ axis is used to define the energy potential that imposes orientational order on the

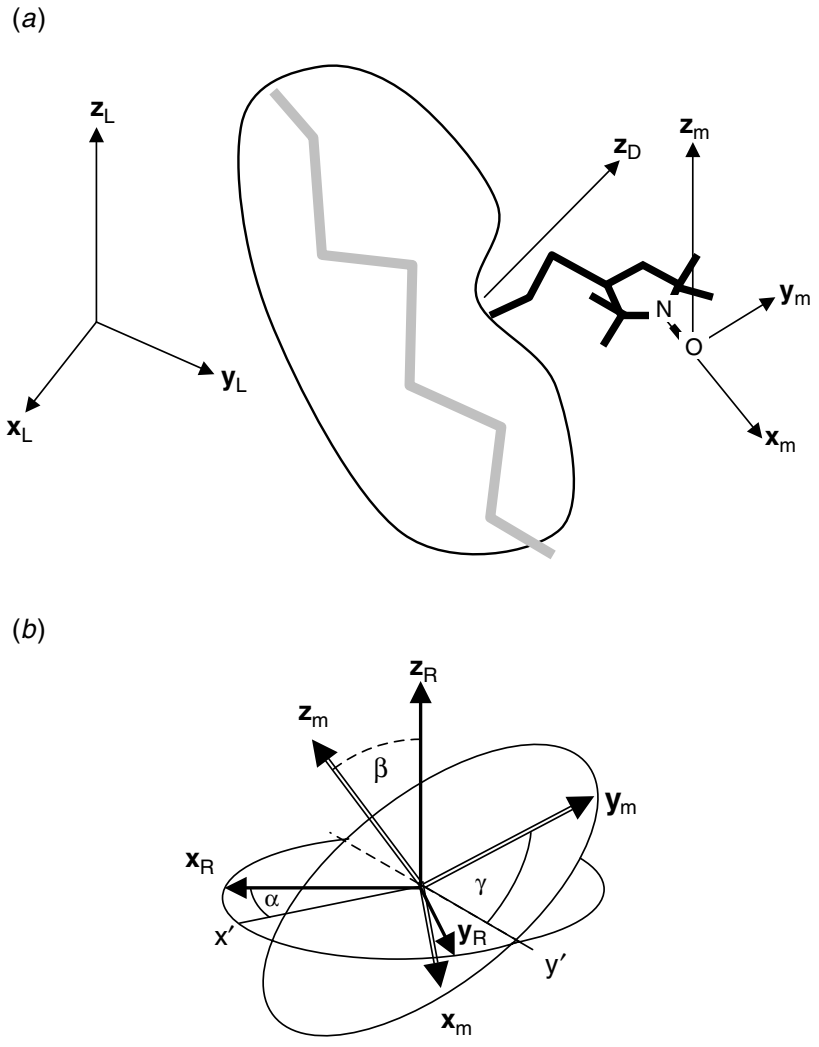

Fig. 6. (*a*) Different coordinate systems (laboratory: L, director: D, and magnetic: m) used to define motion parameters for a nitroxide spin label. (*b*) Diffusion rotation angles used to define the magnetic axes relative to the diffusion axes. Note that the reference system for these angles is the diffusion frame, whereas the reference system is the magnetic (*g*) frame for the magnetic tilt angles (cf. Fig. 3).

probe molecule as described above. The *magnetic frame* ($\mathbf{x}_m$, $\mathbf{y}_m$, $\mathbf{z}_m$) already defined above is fixed relative to the structure of the nitroxide label. Another important frame is the principal axis system of the rotational diffusion tensor, or *rotational diffusion frame* ($\mathbf{x}_R$, $\mathbf{y}_R$, $\mathbf{z}_R$), which is fixed relative to the magnetic frame. The orientations of the principal diffusion axes are specified by the *diffusion tilt angles* $\Omega_D = (\alpha_D, \beta_D, \gamma_D)$, which are the Euler angles of the magnetic axes in the rotational diffusion frame as defined above. These Euler angles are defined in exactly the same way as those shown in Fig. 3 and the accompanying discussion. However, it is important to note that the base frame for the magnetic tilt angles is the magnetic (*g*-tensor) axis system, whereas the base frame for the diffusion tilt angles is the diffusion axis system (cf. Fig. 6*b* with Fig. 3), even though both sets of angles involve the magnetic frame.

The standard model for diffusive motion in polymers is Brownian diffusion, which occurs as a series of infinitesimal reorientational steps. This model is most appropriate for intermediate-to-large sized spin probes and spin-labeled macromolecules, where the macromolecule is much larger than any solvent molecules. Because of this broad applicability, the Brownian diffusion model is the most widely used. This type of rotational diffusion is completely analogous to the one-dimensional random walk used to describe translational diffusion in standard physical chemistry texts, with the difference that the steps are described in terms of a small rotational step $\delta\theta$ that can occur in either the positive or negative direction. In three dimensions, rotations about each of three principal axes of the nitroxide must be taken into account. A diffusion constant may be defined for each of these rotations motions, in a way that is completely analogous to the definition of translational diffusion constant for the one-dimensional random walk.

The orientations of the principal diffusion axes $\mathbf{x}_R$, $\mathbf{y}_R$, $\mathbf{z}_R$ depend critically on the hydrodynamic properties and geometry of the spin label as well as its attachment to the polymer backbone. The rotational diffusion constants R_x, R_y, and R_z associated with each axis are in general different from each other; however, nitroxides that are covalently tethered to a polymer backbone generally exhibit a principal rotation axis, around which the probe rotation is significantly faster than for any other axis. This principal direction is assigned to be the z_R axis and its orientation is typically determined by the tether bonds of the nitroxide to the polymer backbone.

In cases where the overall rotation of a polymer molecule may be neglected because of its size, the combined motion of the spin label and local polymer chain segment may be approximated using a single rotational diffusion tensor.[19,20] This approximation assumes that the local polymer chain segment has an isotropic rotational diffusion coefficient R_S and the spin label rotates with diffusion coefficient R_I around the tether by which it is attached to the polymer. In this case, the rotational diffusion tensor will have axial symmetry, with $R_\perp = R_S$ and $R_\parallel = R_S + R_I$.

The EPRLL programs also allow for non-Brownian rotational diffusion, which implies a discrete, step motion of the spin probe. Two limiting models are available: (*1*) jump diffusion, and (*2*) approximate free diffusion. In currently available implementations of the SLE line shape calculation, non-Brownian models may not be used with an orienting potential, and only with the assumption of an axially symmetric diffusion tensor. For these reasons, and since Brownian motion is usually an

excellent approximation for large molecular systems, such models are only rarely applied in the analysis of spin-labeled polymers.

In addition to the rotational diffusion constants $R_{\|} = R_z$ and $R_{\perp} = R_x = R_y$, non-Brownian diffusion around each axis is specified using the *model parameters*, $P_{\|} = R_{\|}\tau_{\|}$ and $P_{\perp} = R_{\perp}\tau_{\perp}$, where $\tau_{\|}$ and $\tau_{\perp}$ are the non-Brownian *residence times*. The physical interpretation of the residence time for a given axis depends on the specific model used. In jump diffusion, the molecule remains stationary for an average time τ after which it jumps to a new orientation, specified by an angle of rotation about the specified axis. The root-mean-square reorientation angle (in rad) is given by the formula $\theta_{avg} = \langle\theta^2\rangle = 6R_i\tau_i$, where i specifies the axis perpendicular or parallel to z_R. In the approximate free diffusion model, the molecule rotates freely about axis i with a rotational rate R_i, but instantaneously reorients at an average interval τ, after which it continues its free rotation. Like all of the other dynamic parameters in the EPRLL family programs, the non-Brownian residence time products are specified on the $\log_{10}$ scale.

In addition to the rotational diffusion models mentioned above, it is possible to account approximately for the effects of isotropic Heisenberg spin exchange between probe molecules with a rate specified by ω_{SS} (in units of rad s^{-1}). This parameter may become important in microscopically heterogeneous polymers, where aggregation of the spin probes is possible, and it has been applied to account for spin–spin interactions of spin labels adsorbed to the surfaces of zeolites.[21,22] In its original implementation, ω_{SS} was used to simulate the line broadening of the fast-motional spectrum that occurs at high-spin probe concentrations, reflecting the encounter rate between spin-bearing molecules. However, the most recent program modification allows exchange to take place between spin labels of arbitrary orientation.[14]

2.3. Orientational Ordering in Spin-Labeled Polymers

The EPRLL programs include a mechanism to describe the tendency of a spin label or spin probe to become partially ordered within its local environment, a situation that is encountered frequently in spin-labeled polymers. Probe ordering is characterized through the use of an orienting potential that governs the tendency of the spin probe to align relative to the polymer molecule. It may also be regarded as imposing constraints upon the spin-label motion, so that the probe samples only a restricted range of orientations as it moves.

The orienting potential was originally intended for use with materials, such as liquid crystals and membranes, where the molecules align with a macroscopic direction called the *director*. In polymer systems, the director is usually defined microscopically, reflecting the fact that local structural features, such as the polymer backbone or microscopic crystalline or liquid-crystalline domains of the polymer, influence the label alignment.

Figure 7 illustrates one way in which the local director may be defined in spin-labeled polymer systems. As the spin label moves relative to the polymer, its diffusion axes trace trajectories in a reference frame that is fixed relative to the polymer. The orientation trajectory may be regarded as a path traced by the vector on the

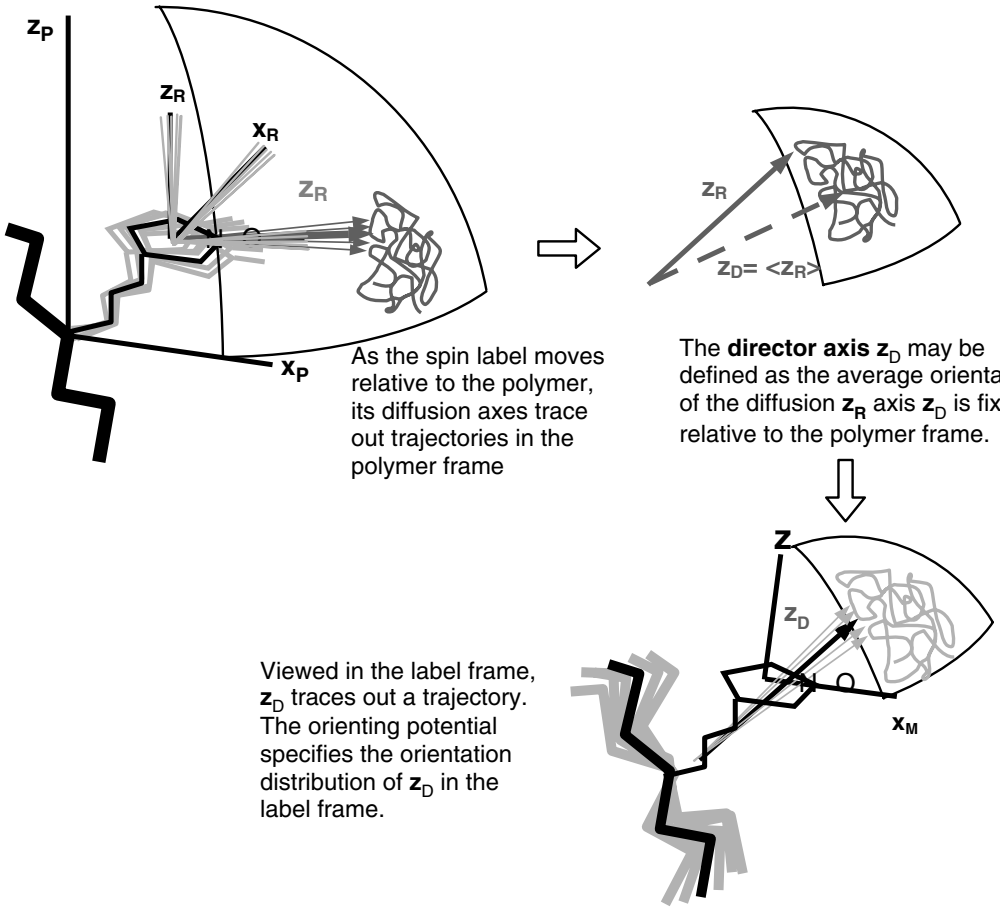

Fig. 7. Definition of the local director axis in spin-labeled polymer systems.

surface of a sphere. The director axis $\mathbf{z}_\mathrm{D}$ may be defined as the average orientation of the diffusion $\mathbf{z_R}$ axis over the course of its motion. The $\mathbf{z}_\mathrm{D}$ vector is thus fixed relative to the polymer frame. However, viewed in the spin-label frame, $\mathbf{z}_\mathrm{D}$ traces a trajectory. The orienting potential specifies the orientation distribution of $\mathbf{z}_\mathrm{D}$ in the rotational diffusion frame.

The orienting potential is expressed as a function of the polar angles (θ,ϕ) of the director in the rotational diffusion axis frame. It is most conveniently included in the SLE equation by expanding it in a series of spherical harmonic functions $\mathcal{D}_K^L$ as follows:

$$U(\Omega) = -\sum_{L,K} c_{LK}\mathcal{D}_K^L(\theta,\phi) = -\sum_{L,K} c_{LK}\left[D_{0K}^{\mathrm{L}}(\theta,\phi) + D_{0-K}^{L}(\theta,\phi)\right] \qquad (2)$$

Each function $\mathcal{D}_K^L$ is a symmetric combination of generalized spherical harmonic functions $D_{0K}^{\mathrm{L}}(\Omega)$, where Ω is the set of Euler angles that specifies the orientation of the director with respect to the label frame. The symmetrical combination of spherical harmonics with $+K$ and $-K$ indices ensures that each of the $D_{0K}^{\mathrm{L}}(\Omega)$ functions (and thus the potential U) is real valued.

The EPRLL-family programs include additional restrictions on the terms in Eq. 2. The summation is restricted to even values of L and K that are ≤ 4. Thus, there are

only five terms in the potential, represented by the coefficients c_{20} , c_{22}, c_{40}, c_{42}, and c_{44}. These restrictions are equivalent to two assumptions about the ordering potential: first, that the orienting potential has at least twofold symmetry, and second, that the principal ordering axes of the nitroxide are identical to the principal diffusion axes. The observables obtained by least-squares analysis of the ESR spectrum are the coefficients c_{LK}, which are expressed as energy in units of *kT*.

The observable effect of an orienting potential upon the ESR spectrum is the anisotropic distribution of orientations produced by the potential. The equilibrium distribution of orientations obeys the Boltzmann relation,

$$P(\theta,\phi) = \frac{\exp\left[-U(\Omega)/kT\right]}{\int_{\Omega}\exp\left[-U(\Omega)/kT\right]d\Omega} \tag{3}$$

where *P* is the probability of finding the director axis z_{D} with polar angles in the diffusion frame between (θ,ϕ) and $(\theta + d\theta, \phi + d\phi)$.

One may obtain some idea about the shapes of the orienting potentials produced by each term in Eq. (2 by recognizing their equivalence with the more familiar shapes of atomic orbitals, which are also based on spherical harmonics. For example, the $L = 2$, $K = 0$ function is similar to the d_z^2 orbital, with a positive lobe along the $+z$ direction and a negative lobe in the *xy* plane, perpendicular to *z*. Likewise, the $L = 2$, $K = 2$ corresponds to the $d_{x^2-y^2}$ orbital. Each of the possible terms in the orienting potential function is given with its explicit functional form and the related atomic orbital designation in Table 2. The corresponding population distributions $P(\theta,\phi)$ for each function are displayed in Fig. 8. Two columns are shown for the two possible signs of the coefficient for each function in order to emphasize the regions for which the function is positive or negative. Figure 8 makes apparent that the orienting potential and related population distribution function refer to the distribution of the director in the label diffusion frame. For example, the $L = 2$, $K = 0$ function has a positive lobe along the $\mathbf{z}_{\mathrm{R}}$ axis and a negative lobe or ring in the $\mathbf{x}_{\mathrm{R}}$ - $\mathbf{y}_{\mathrm{R}}$ plane. Thus, a potential

TABLE 2. Terms in the Energy Potential Used to Describe Spin Label Orientation

Term	Functional Form	Analogous Atomic Orbital
$\mathcal{D}_0^2(\theta)$	$\frac{1}{2}(3\cos^2\theta - 1)$	d_{z^2}
$\mathcal{D}_2^2(\theta,\phi)$	$\sqrt{\frac{3}{2}}\sin^2\theta\cos 2\phi$	$d_{x^2-y^2}$
$\mathcal{D}_0^4(\theta)$	$\frac{1}{8}[(35\cos^2\theta - 30)\cos^2\theta + 3]$	g_{z^4}
$\mathcal{D}_2^4(\theta,\phi)$	$\sqrt{\frac{5}{8}}\sin^2\theta(7\cos^2\theta - 1)\cos 2\phi$	$g_{z^2(x^2-y^2)}$
$\mathcal{D}_4^4(\theta,\phi)$	$\sqrt{\frac{35}{8}}\sin^4\theta\cos 4\phi$	$g_{x^4-y^4}$

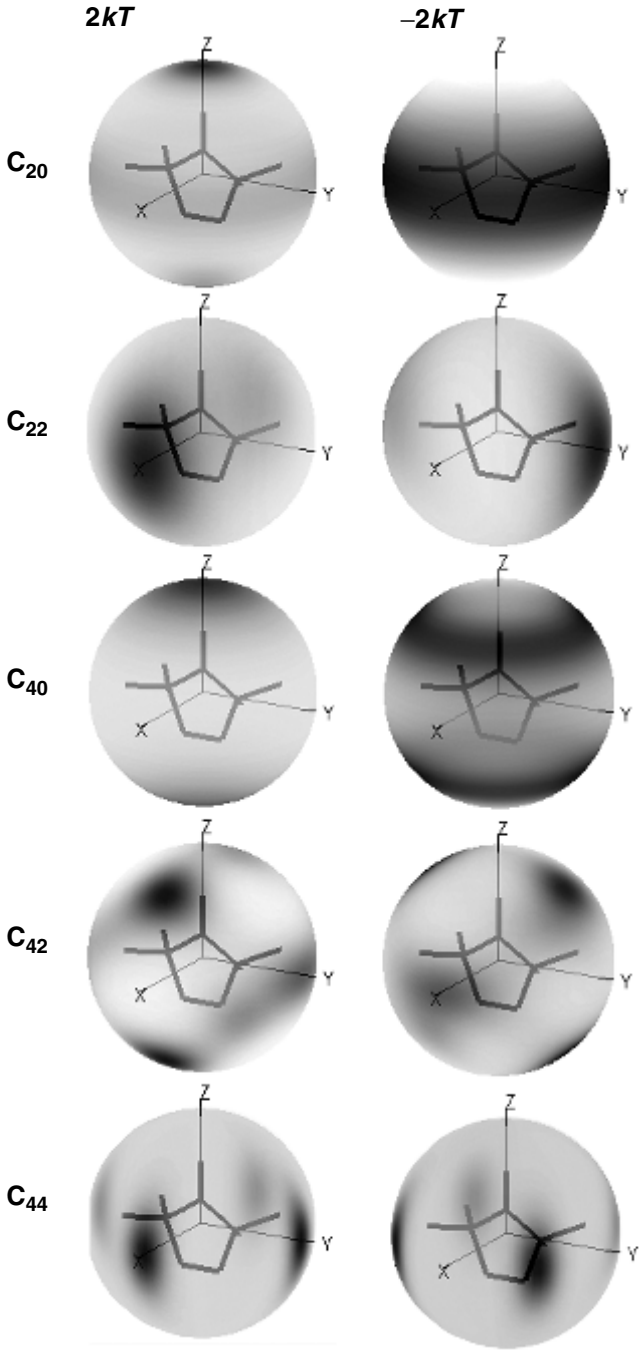

Fig. 8. Population distributions $P(\theta,\phi)$ calculated for each of the functions used in the orienting potential expansion given in Table 2.

with a positive c_{20} coefficient will have a minimum for $\theta = 0$ (i.e., along the $\mathbf{z}_R$ axis) by virtue of the negative sign in Eq. 2. In turn, this will produce a maximum in the orientation population distribution at this orientation according to the Boltzmann relation in Eq. 3, as shown in the top plot on the left-hand side of Fig. 8. In contrast, a negative c_{20} will produce a minimum in the potential at $\theta = 90$, leading to a maximum in the director orientation distribution in the $\mathbf{x}_R$ - $\mathbf{y}_R$ plane, as shown in the top plot on the right-hand of Fig. 8. By analogy, the $L = 2$, $K = 2$ function has positive lobes along

the $\mathbf{x}_R$ axis and negative lobes along the $\mathbf{y}_R$ axis, so that a positive c_{22} coefficient produces director orientations distributed along $\mathbf{x}_R$ and a negative c_{22} produces orientations along $\mathbf{y}_R$ (*cf.* plots second from the top in Fig. 8). Similar arguments apply to the higher order functions shown in the figure.

In practice, satisfactory fits to experimental ESR spectra at 9 GHz can usually be obtained by varying only the c_{20} and c_{22} coefficients. However, higher frequencies afford greater orientational resolution, so that higher order terms in the potential are often required to achieve satisfactory fits to high-frequency spectra. Even within the limitations placed on the orienting potential function expansion, the distributions in Fig. 8 make clear that rather complex orientation distributions can be reproduced by an appropriate combination of potential coefficients. Figure 9 illustrates two of the more commonly encountered distribution shapes that reflect potentials with significant contributions from at least two of the functions given in Table 2.

The first commonly encountered distribution is an "elongated spot" shown along the top of Fig. 9, which arises from combinations of the c_{20} and c_{22} coefficients. This type of distribution is observed when the probe experiences different degrees of orientation around different axes, as depicted schematically in the cartoon in Fig. 10*a*. Assuming that z is the ordering axis as shown in Fig. 9, the direction of the elongation

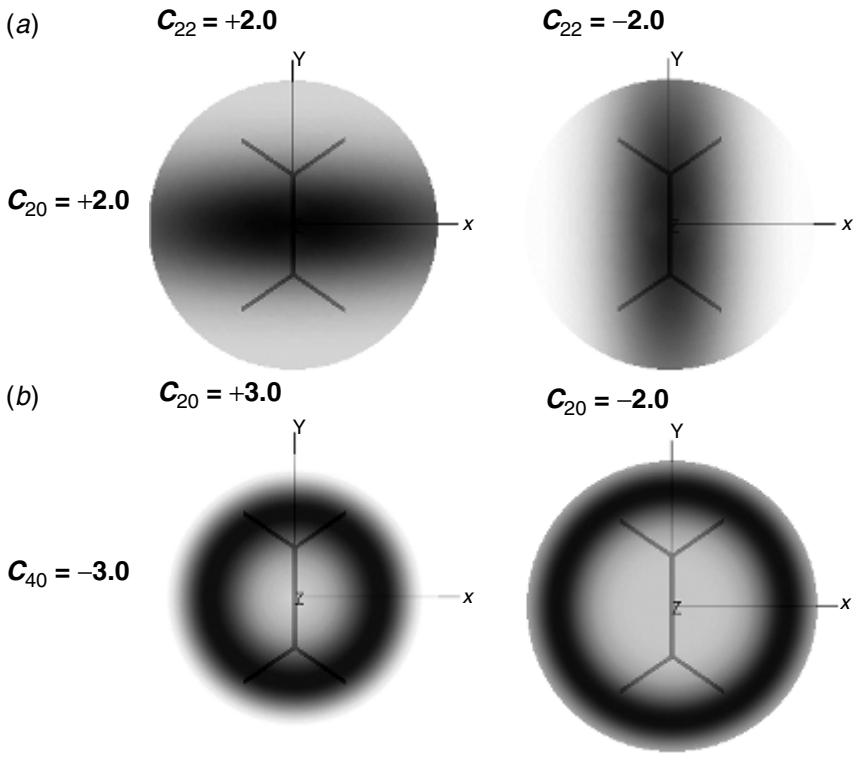

Fig. 9. Two commonly encountered shapes of director axis distributions relative to the nitroxide frame, given by potentials with significant contributions from at least two of the functions given in Table 2. (*a*) Elongated spot given by different combinations of the c_{20} and c_{22} coefficients; note that the orientation of the long axis of the spot depends on the sign of c_{22}. (*b*) Cone distributions given by different combinations of the c_{20} and c_{40} coefficients, with $c_{40} < 0$. The angle of the cone is determined by the ratio c_{40} / c_{20}.

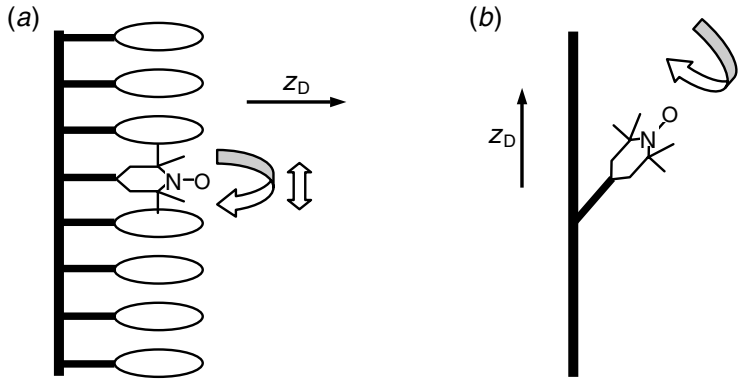

Fig. 10. Cartoons depicting situations in which a spin-labeled polymer may yield the types of local director distribution shapes shown in Fig. 9. (*a*) Director perpendicular to polymer chain direction, determined by interactions between spin-label and liquid-crystalline side chains. Different ordering around two axes leads to the elongated distributions shown at the top of Fig. 9*b* Director parallel to main-chain direction, with spin label held at a fixed angle with respect to the chain, leading to the conical distributions shown at the bottom of Fig. 9.

is determined by the sign of c_{22}: for positive c_{22}, the spot is elongated in the xz plane, and for negative c_{22}, it is elongated in the yz plane. Appropriate combinations of c_{20} and c_{22} can be used to produce the same distribution with x or y as the ordering axis. Barnes and Freed have given a useful set of relations that can be used to accomplish these transformations.[23]

A second commonly encountered distribution is the cone distribution illustrated along the bottom of Fig. 9, and in Fig. 10*b*. This type of distribution is produced by a combination of the c_{20} and c_{40} coefficients, with $c_{40} < 0$. The half-angle of the cone is determined by the ratio of c_{20} and c_{40} as follows:

$$\cos^2\theta_{\text{cone}} = \left(\frac{3}{7} - \frac{6}{35} \frac{c_{20}}{c_{40}} \right) \tag{4}$$

Although c_{40} must be negative to obtain a conical distribution, c_{20} is positive for $\theta_{\text{cone}} < 49.1$, and negative for $\theta_{\text{cone}} > 49.1$. Any half-angle between 0 and 90 can be modeled in this way, which enables one to model most situations of practical interest in spin-labeled polymers.

In the presence of an orienting potential, another model for spin-label diffusion that is available from the EPRLL family programs is the "anisotropic viscosity" model, originally described by Polnaszek et al.[24] The anisotropic viscosity model is primarily used for macroscopically ordered fluids such as membranes and liquid crystals and its applicability to spin-labeled polymer systems is limited to cases where the polymer may be aligned macroscopically to a relatively high degree of order. The dynamic model that is most commonly applied to polymers in the presence of a local orienting potential is some form of the microscopic order–macroscopic disorder (MOMD) model described in Section 2.4.

2.4. The Microscopic Order–Macroscopic Disorder Model

In most cases, the local directors in a polymer sample are not aligned with each other, and therefore cannot be aligned with a macroscopic direction. That is, the polymer sample consists of locally ordered domains that are randomly oriented with respect to the laboratory frame as illustrated schematically in Fig. 11. The model describing this situation is known as the MOMD model. As originally described for spin-labeled biological membranes and proteins,[25] the model assumes that the spin probe undergoes microscopic molecular ordering with respect to a local director; however, the local directors in the sample are randomly oriented and rigidly fixed with respect to the laboratory frame. This situation is realized in many types of polymers with crystalline or liquid-crystalline phases, and may also apply to spin labels where the local dynamics is constrained by the tether bond or by interaction with polymer side chains.

The approach to calculating a MOMD spectrum using the EPRLL programs is straightforward: The spectrum must be integrated over the distribution of local director orientations Ψ. Figure 12 shows the component spectra corresponding to selected tilt angles that are integrated to give MOMD spectra at both 9 and 94 GHz. In the calculation program, a MOMD spectrum is specified simply by setting the number of tilt angles orientations, n_{ort}. It is important to allow enough tilt angles to ensure proper sampling of director orientations and convergence of the MOMD spectrum. At 9-GHz frequencies, between 10 and 30 orientations are generally needed, with a

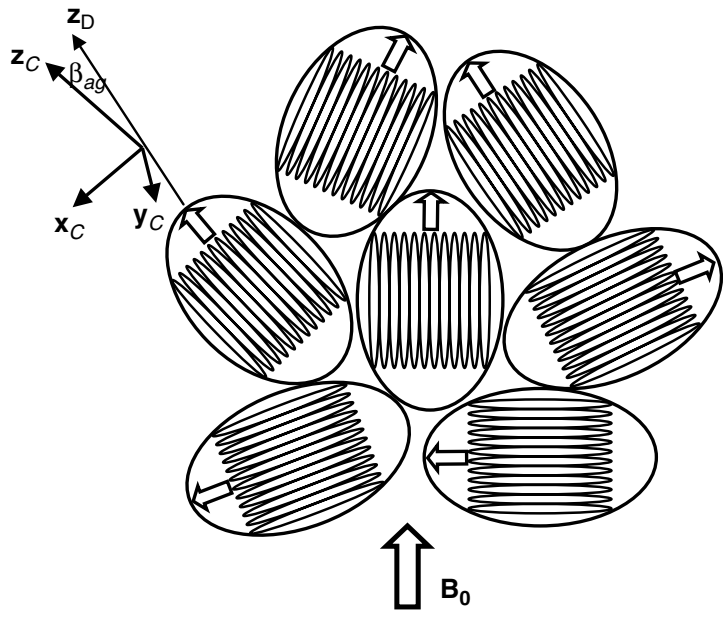

Fig. 11. A representation of a MOMD sample showing local ordering of microdomains with directors $\mathbf{z}_D$ (heavy arrows), but macroscopic disorder due to the random orientations of the microdomains in a three-dimensional disordered 'mosaic'. The applied magnetic field $\mathbf{B}_0$ points along the laboratory $\mathbf{z}$ axis. The upper left shows the axis system defined for the case of a slowly relaxing local structure. Motion of the microdomains is defined relative to the "cage" system $\mathbf{x}_C$, $\mathbf{y}_C$, $\mathbf{z}_C$, and β_{ag} is the tilt angle between the principal cage diffusion axis $\mathbf{z}_C$ and the local director $\mathbf{z}_D$.

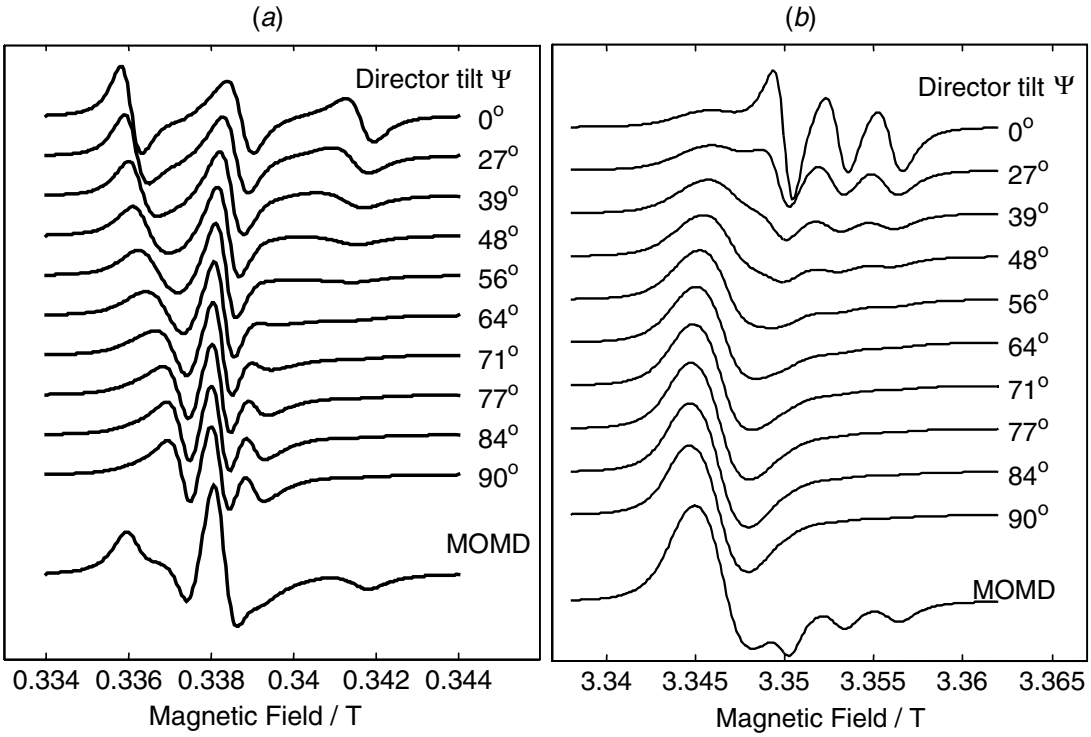

Fig. 12. Components of a MOMD ESR spectrum of a nitroxide spin label, showing the individual spectra from domains with different tilt angles, and integrated MOMD spectrum at the bottom, for 9 GHz (left-hand side) and 94 GHz (right-hand side).

greater number of orientations required when the line width for a single orientation is small. More orientations are also required at higher frequencies, where the orientation resolution is greater.

The EPRLL family programs also admit a "partial MOMD" model described by Barnes and Freed.[23] This model includes microscopic ordering with respect to a local director just as in the MOMD model; however, the directors are assumed to be partially ordered with respect to a macroscopic ordering axis. The tilt angle Ψ in this case refers to the angle between the spectrometer field and the macroscopic ordering direction. The macroscopic ordering is described by a potential that is analogous to the microscopic spin-label ordering potential; however, it only includes the $L = 2$, $K = 0$ term with coefficient b_{20}. Although the partial MOMD model was originally conceived to treat partially ordered membrane dispersions, it should be applicable to such systems as spin-labeled polymer fibers that are partially aligned with a macroscopic direction.

The dynamic parameters for the EPRLL program are summarized and defined in Table 3.

2.5. Slowly Relaxing Local Structure Model

A more general dynamic model permits motion of the potential-defining environment on the ESR time scale, as might occur in a slowly tumbling spin-labeled polymer. In such a system, the ordering potential is considered to define the constrained

TABLE 3. Dynamic Parameters of EPRLL Programs

Symbol	Name	Description
α_D, β_D, γ_D	**alphad, betad, gammad**	Diffusion tilt angles in degrees
c_{20}, c_{22}, c_{40}, c_{42}, c_{44},	**c20, c22, c40, c42, c44**	Orienting potential coefficients in units of kT
b_{20}	**b20**	Director orienting potential coefficient for $L=2$, $K=0$ in units of kT
ω_{ss}	**oss**	Log_{10} of Heisenberg spin exchange rate in sec^{-1}
$P_\perp$, $P_\parallel$	**pmxy, pml**	Model parameter for non-Brownian motion around z axis
Ψ	**psi**	Director tilt angle in degrees
$\underline{R}_x$,R_y, R_z	**rx, ry, rz**	Cartesian (and spherical) components of the rotational diffusion tensor ($\log_{10}$ of diffusion constant in s^{-1})
R, N, N_{xy}	**rbar, n, nxy**	
$\hat{R}_\parallel$, $\hat{R}_\perp$	**djf, djfprp**	Anisotropic viscosity rotational diffusion rate constants parallel and perpendicular to director

environment of the tethered spin probe. This constrained environment slowly reorients with respect to the laboratory frame as the polymer tumbles in solution, providing the coupling to the over-all, or global, diffusion.

The slowly relaxing local structure (SRLS) model describes this type of composite dynamics using only a few modes of diffusion. The main justification for this simplification is the limited resolution of the observed ESR line shapes. In the SRLS model, the spin probe is assumed to be reorienting in a local environment that is relaxing on a longer time scale. In applications to macromolecular systems, the faster motion describes the internal dynamics, while the slower motions account for the global rotation of the macromolecule.

It is important to note that the SRLS model contains the MOMD model as a limiting case, namely, the rigid limit for the slower global motion. Another significant limiting case occurs when the internal dynamics is in the fast-motion limit, called fast internal motion (FIM) model. In the FIM model, the internal dynamics lead to a partial averaging of the magnetic tensors, which is quantified by an effective-order parameter. The rotational diffusion tensor then describes the global motion.[26]

The general SRLS model requires a number of additional parameters to describe the global diffusion modes.[27–29] Three rotational diffusion constants, R_x^0, R_y^0, and R_z^0 are used to characterize the reorientation of the SRLS cage. They are expressed on the

$\log_{10}$ scale, and may be expressed as the pseudo-spherical components $\overline{R}^0$, N^0, and N^0_{xy} by analogy with the probe diffusion parameters described above. Finally, the general SRLS model includes a tilt angle β_{ag} between the principal cage diffusion axis $\mathbf{z}_C$ and the local director $\mathbf{z}_D$. The SRLS dynamic parameters are summarized in Table 4.

Often, a simplified SRLS model is sufficient to describe experimental data. Most commonly, only one additional dynamical parameter, $R^C_\perp$, is needed to describe the cage diffusion. Also, the mean-field cage potential can often be approximated with cylindrical symmetry, so that only the $L = 2$ parameters need be retained in the cage orienting potential.

Although the SRLS model has not yet been extensively applied to spin-labeled polymer systems, there are a number of studies on model and biological systems that illustrate its potential utility in this application. SRLS is needed in cases where both the local and global dynamics induce significant averaging of the spectrum. For example, time scales typical of global macromolecular modes of motion generally fall within the slow-motion regime near ESR frequencies of 9 GHz; thus, it is important to account for both the global and local dynamics at this frequency. In contrast, the global modes of motion are often in the rigid limit at high ESR frequencies. Thus it is possible to determine local dynamic parameters using the MOMD model at high frequency, then fix these parameters in a constrained SRLS analysis of 9-GHz spectra to characterize the global dynamics. The work of Liang and Freed, who derived the MOMD limit from the more general SRLS model,[26] validated this general approach.

The SRLS mechanism has been invoked to explain the segmental rotational dynamics of spin-labeled polystyrene in toluene solution.[20] This study provides an example of a system in which the dynamic cage is defined by constrained diffusion of the spin label attached to a polymer. The SRLS model is appropriate to analyze these spectra, since the local ordering environment is coupled to the global tumbling modes of the polymer. Moreover, the high (250–GHz) frequency ESR spectra of this

TABLE 4. SRLS Parameters of ESR Line Shape Programs

Symbol	Name	Description
a_{20}, a_{22}, a_{40}, a_{42}, a_{44}	**a20, a22, a40, a42, a44**	Coefficients of coupling potential between SRLS cage and spin probe in units of kT
b_{10}, b_{20}	**b10, b20**	Coefficients of orienting potential for SRLS cage in units of kT
$\underline{R}_x{}^o$, $R_y{}^o$, $R_z{}^o$ R^o, N^o, $N_{xy}{}^o$	**r0x, r0y, r0z r0bar, n0, n0xy**	Cartesian (and spherical) components of the rotational diffusion tensor for the SRLS cage ($\log_{10}$ of diffusion constant in s^{-1})
β_{ag}	**bag**	Cage tilt angle between the SRLS cage principal diffusion axis and the SRLS cage director

system are not sensitive to the global tumbling modes of the polymer, as they are too slow on the 250-GHz ESR time scale.

3. OTHER STOCHASTIC LIOUVILLE CALCULATION PARAMETERS

This section describes a number of input parameters used to control the stochastic Liouville calculation itself, the most notable of which are the parameters that specify the basis set used to carry out the calculation.

3.1. Basis Set for the Stochastic Liouville Calculation

The solution of the SLE may be expressed as the following matrix equation:

$$I(\Delta\omega) = \langle\langle v|[(-i\mathbf{L}+\Gamma)+\mathbf{I}\Delta\omega]^{-1}|v\rangle\rangle \tag{5}$$

in which I is the intensity of the spectrum, ω is the frequency, $\mathbf{L}$ is the Liouville superoperator that governs the quantum mechanical evolution of the electron and nuclear spins, Γ is the stochastic superoperator that governs the spin probe motion, $\mathbf{I}$ is the unit matrix, and v is a vector that projects out the observable magnetization and equilibrium orientation distribution of the probe. Although we will not go into the details of this calculation, it is necessary to understand a few important features of Eq. 5 in order to apply it to ESR line shape analysis.

The most important feature of the matrices and vectors in Eq. 5 is that they are constructed in a vector space, or *basis set*, that consist of the direct product of generalized spherical harmonic functions representing the rotational degrees of freedom of the probe, and spin functions that represent its spin degrees of freedom. Proper specification of the basis set is therefore an important requirement for accurate calculation of the slow-motional spectrum.

Each basis function in the EPRLL program is specified by five quantum numbers: L, K, M, p_I, q_I, with L, K, and M specifying the generalized spherical harmonic function, and the transition indices p_I and q_I specifying the spin functions. Note here that p_I and q_I refer only to nuclear spin states. In the general formulation of the SLE, it would also be necessary to include the indices p_S and q_S for the electronic spin states; however, the EPRLL programs make use of the high-field approximation, which implicitly restricts the calculation to the $p_S = 1$, $q_S = 0$ subspace.[13] The basis set indices and the physical quantities they represent are summarized in Table 5.

We briefly mention that, for the SRLS model described above, up to three additional basis indices are needed to represent motion of the solvent cage, namely, L^C, K^C, and M^C. These indices are specified by truncation parameters and have the same general physical meaning (in the context of cage diffusion) as the L, K, and M indices in Table 5. The different approaches to optimizing basis sets described in Sections 3.2 and 3.3 also apply to the cage indices; however, for the sake of simplicity, the SRLS model in these sections will not be considered.

TABLE 5. Basis Set Indices and Their Physical Interpretations

Index	Physical Interpretation	Range
L	Quantum number for total rotational angular momentum	(0 to L_{emax})
K	Quantum number for projection of rotational angular momentum on laboratory Z axis	($-L$ to L)
M	Quantum number for projection of rotational angular momentum on molecular Z axis	($-L$ to L)
p_{I}	Nuclear spin transition index: net change in Z projection of nuclear magnetic moment	($-2I$ to $2I$)
q_{I}	Nuclear spin transition index: total number of nuclear spin quanta involved in a transition	($\lvert p_{\mathrm{I}}\rvert - 2I$ to $2I - \lvert p_{\mathrm{I}}\rvert$)

3.2. Basis Set Symmetrization

The full basis set of basis functions used in the SLE calculation includes both positive and negative K and M indices. However, the entire range of indices is required only in the general case; in many cases of interest, it is possible to reduce the number of K and M values in the basis set. This reduction is accomplished by two so-called "symmetrization" transformations called the K and M symmetrizations. To illustrate what this means, the K-symmetrized basis set is constructed by taking symmetric and antisymmetric combinations of basis functions with the same absolute value of K. That is, each pair of functions $\left|L, K, M, p^I, q^I\right\rangle$ and $\left|L, -K, M, p^I, q^I\right\rangle$ in the original basis are used to form two new functions proportional to $\left(\left|L, K, M, p^I, q^I\right\rangle \pm \left|L, K, M, p^I, q^I\right\rangle\right)$. The new functions are specified by their (non-negative) K index and a symmetry index j^K, which is $+1$ for the symmetric and -1 for the antisymmetric combination. The M symmetrization is similar, although this transformation also includes specific combinations of spin transition indices.[13,14]

Although the K and M indices are always non-negative in the symmetrized basis, the EPRLL programs accept negative values for the K and M truncation indices, using the convention that negative K or M values specify j^{K} or $j^{\mathrm{M}} = -1$. Many typical SLE calculations do not require basis functions with j^K or $j^M = -1$. The special circumstances requiring use of negative K and M indices are discussed below.

3.3. Basis Set Truncation Parameters

For any of the basic EPRLL-family programs, it is necessary to specify the range of basis set indices that will be used to construct the SLE matrix equation. This is done via the five *truncation parameters*, L_{emx}, L_{omx}, K_{mx}, M_{mx}, and $p^{\mathrm{I}}{}_{\mathrm{mx}}$, which specify the maximum values that may be assumed by each quantum number in the basis. Separate maxima are specified for even and odd L values, and no truncation parameter is

needed for the q_I index. In cases where negative K and M indices are required, two additional truncation parameters are also used: K_{mn} and M_{mn}.

In general, higher truncation values are needed to represent slower motions. This may be understood by the following analogy. A rigid limit ESR spectrum is calculated by averaging the spectrum over all possible orientations of the paramagnetic species relative to the spectrometer field. It is therefore necessary to sample the orientations with sufficient resolution to achieve a smooth line shape; an insufficient number of orientations produces "ripples" in the line shape. By analogy, higher L, K, and M indices correspond to sampling of a larger number of orientations. Thus, if the truncation indices used for a given slow-motional calculation are not large enough, "ripples" appear in the calculated slow-motional spectrum, as shown in Fig. 13.

Since the matrix size, and thus the processor time, for a given calculation increase geometrically with the truncation indices, calculations can quickly become quite time-consuming as the basis set is increased. Thus, it is desirable to optimize the basis by finding the smallest set necessary for acceptable convergence of the calculated spectrum, particularly for MOMD spectra. When the truncation parameters are all set to their respective acceptable minima, the corresponding list of basis elements is referred to as the *minimum truncation set* (MTS), and the truncation parameters are called the MTS parameters.

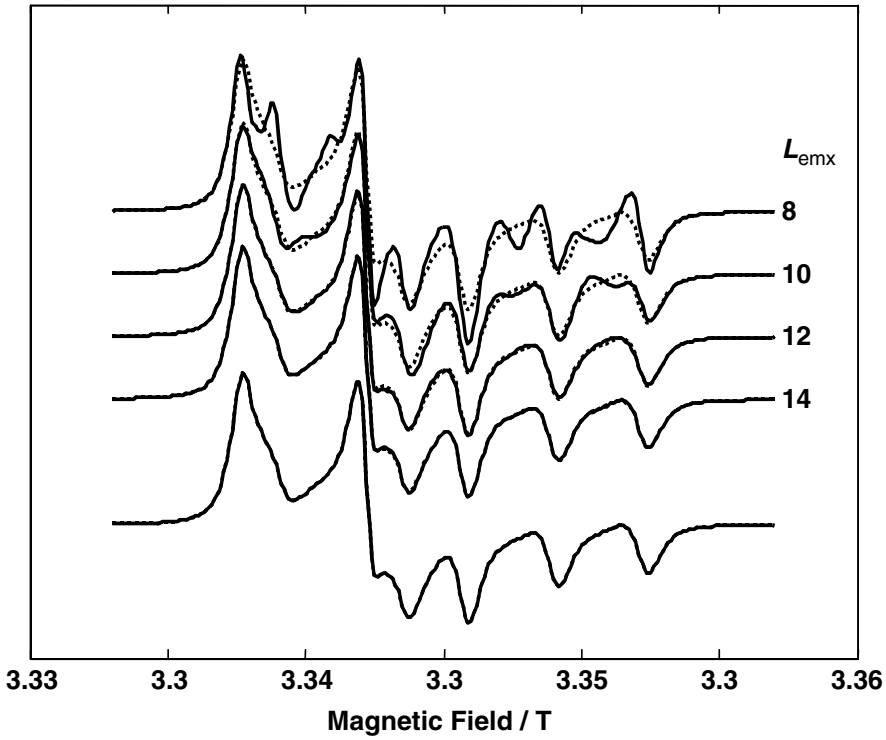

Fig. 13. Effects of using an incomplete basis set on the calculated slow-motional 94 GHz ESR spectrum of a nitroxide. The converged spectrum calculated with $L_{emx} = 22$ is shown at the bottom, and by the dashed lines above. Spectra calculated with indicated maximum L-index (L_{emx}) values are shown by dashed lines and compared with the converged spectrum. Note the appearance of significant oscillations in the spectrum as L_{emx} decreases.

3.4. Guidelines for Selecting Basis Set Truncation Parameters

This section gives some rules of thumb for selecting MTS parameters to optimize the speed of a given slow-motional line shape calculation. They are intended as an approximate guide rather than a definitive set of rules, since the MTS needed for each problem may be slightly different. In general, the reader is recommended to use the basis set "pruning" procedure described below if optimal calculation efficiency is desired. With the availability of fast modern processors, it is often unnecessary to optimize the basis set to the greatest possible extent. Particularly for applications in least-squares fitting, it is desirable to balance computational efficiency with the overhead of having to reoptimize the basis set when the model parameters change significantly.

As mentioned in the last section, the L and K truncation parameters must in general be increased as the motion slows. If the calculation involves an ordering potential with nonzero director tilt angles (including MOMD spectra), the M truncation parameter must also be increased. Separate maxima are specified for even and odd L values. The reason for this is that the number of odd L values required depends on the symmetry of the system: in general, no odd L values are needed at all in the case of axial symmetry, and higher odd values are required as systems deviate further from axial symmetry.

The basic strategy recommended for obtaining appropriate MTS parameters is therefore to start by determining L_{emx} according to the ESR frequency and anticipated minimum $R_\perp$ diffusion parameter. One may then set the remaining parameters (L_{omx}, K_{mx}, and M_{mx}) relative to the L_{emx} value. Figure 12 shows the L_{emx} value obtained over a range of rotational rates for three different ESR frequencies using the swept-fields conjugate gradient method introduced by Vasavada et al.[30] and described below in the section on basis set pruning.

The curves shown in Fig. 14 were calculated from empirical expressions that can be used to estimate the L_{emx} needed for a given calculation from the ESR frequency and $R_\perp$ without performing a swept-fields calculation. Although an axial diffusion tensor was assumed in deriving these expressions, the method may also be applied when a rhombic ($R_{\mathrm{x}} \neq R_{\mathrm{y}}$) diffusion tensor is anticipated, using the lesser of the quantities R_{x}, R_{y}.

The expressions used to calculate the curves shown in Fig. 14 are obtained as follows. First, the value of $\log_{10} R_\perp$ corresponding to the onset of the fast-motion regime is approximated as $\log_{10} R_{\perp,\max} = 8.40 + 0.00745\nu$, where ν is the frequency in gigahertz (GHz). Above this value, $L_{\mathrm{emx}} = 2$ is sufficient to calculate the spectrum. For lower values of $R_\perp$, the plotted curves are calculated for $\nu = 9$, 94, and 140 using Eq. 6,

$$L_{\mathrm{emx}} = A(\nu)\left(\log_{10} R_{\perp,\min} - \log_{10} R_\perp\right)^2 + 2 \tag{6}$$

where A is a frequency-dependent constant given by $3.07 + 0.00679\nu$ (where ν again is in units of GHz). The parameter L_{emx} should be rounded to the next highest even integer above the value returned by this equation.

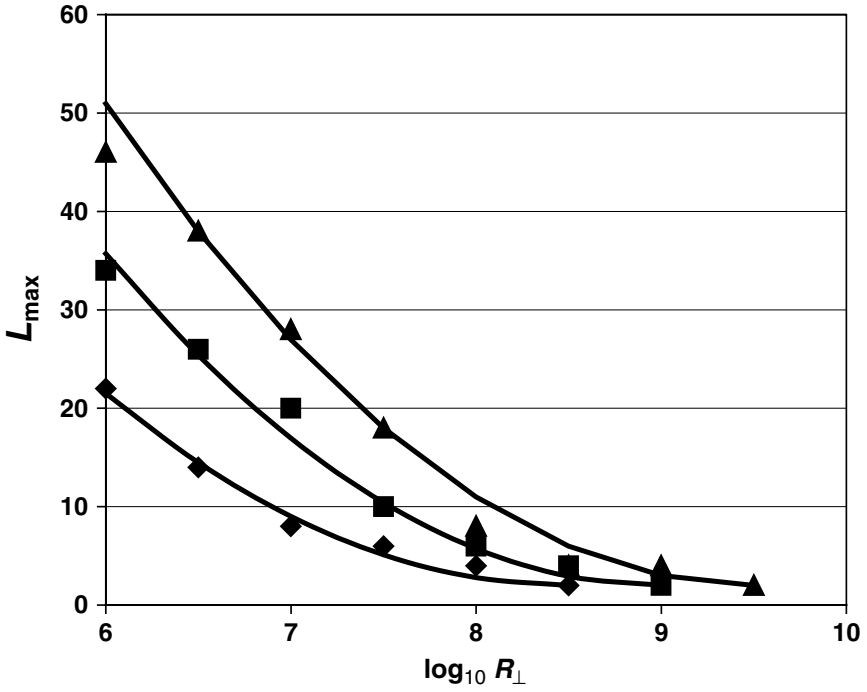

Fig. 14. The L_{emx} values required for convergence of the slow-motional ESR spectrum of a nitroxide as a function of $\log_{10}R_\perp$ at frequencies of (◆) 9 GHz (□) 94 GHz, and (▲) 140 GHz. The L_{emx} values were obtained using the swept-fields calculation of Vasavada et al.[34] with a tolerance of 0.003. Solid lines show empirical functions used to estimate L_{emx} as described in the text.

Once L_{emx} is determined, the appropriate values of L_{omx} and K_{mx} may be set relative to it. For most nitroxide spectra, $L_{omx} = 0.7\ L_{emx}$ (rounded to the next highest odd integer) is sufficient, although this factor can be reduced somewhat at frequencies at or < 9 GHz, where the spectrum is dominated by the nearly axial ^{14}N hyperfine anisotropy. The ratio between K_{mx} and L_{emx} depends on the rotational anisotropy parameter N. For an isotropic rotational diffusion tensor, it is generally sufficient to take $K_{mx}=0.6\ L_{emx}$; when $N \geq 10$ ($\log_{10} N \geq 1$) one may generally use $K_{mx}=0.3\ L_{emx}$; and when $N \leq 0.1$ ($\log_{10} N < -1$) it is necessary to use $K_{mx} = 0.9\ L_{emx}$, in each case rounding to the next highest even integer.

In the absence of an orienting potential, or for zero director tilt in the presence of a potential, M_{mx} may be taken equal to the p^I_{max} value. For MOMD calculations, it is recommended simply to set M_{mx} equal to K_{mx}.

The K_{mn} index should be set to zero unless either the α_D or the γ_D diffusion angle is nonzero. For relatively small tilt angles, only small negative values of K_{mn} are required; however, for angles approaching 45 , K_{mn} should be chosen equal to $-K_{mx}$. In this case, $|K_{mn}|$ and $|K_{mx}|$ may be reduced by a factor of ~0.7 relative to the optimal K_{mx} in the absence of tilt. If the tilt angles are to be varied in a least-squares procedure, however, it is best not to reduce the magnitude of K_{mx} and K_{mn}.

The M_{mn} parameter should generally be set to zero unless there is a significant nuclear Zeeman interaction present. Even in this case, only small negative values of M_{mn} will be needed; however, since the optimal index should depend on the relative

magnitudes of the nuclear Zeeman and nuclear hyperfine interactions, the most reliable way to set M_{mn} is to use the basis set pruning method described below.

The nuclear transition index p^{I} varies from $-\boldsymbol{p}^{\boldsymbol{I}}_{\mathbf{mx}}$ to $+\boldsymbol{p}^{\boldsymbol{I}}_{\mathbf{mx}}$. It is recommended always to set p^{I}_{mx} equal to twice the total nuclear spin ($2I$). Although the larger values of p^{I} are not needed for the very fastest motions, calculations for nitroxides in this motional regime are already rapid enough that eliminating unneeded p^{I} values results in very little savings in computation time.

3.5. Basis Set Pruning

Practical experience has shown that significant reduction of the basis set below that specified by the MTS is possible. That is, not every member of a MTS is needed for a given calculation. However, the pattern of omissions is rather irregular and cannot easily be formulated as a simple set of rules. The alternate strategy implemented in the EPRLL family of programs is simply to keep a list of all the important basis indices using a strategy called "pruning", which has been described in detail.[30]

To prune a basis set, one determines "weighting factors" for each vector in an oversized basis set by finding the maximum of the projection of the basis vector on the solution vector evaluated at a selection of fields across the spectrum. This is done by rearranging Eq. 5 and solving the matrix equation $(i\Delta\omega\mathbf{I} + \Gamma - i\mathbf{L})|u\rangle = |v\rangle$ using a given value of $\Delta\omega$ to obtain a solution vector $|u\rangle$. This calculation is repeated for a number of $\Delta\omega$ values that span the spectrum (typically ≈ 20 at 9 GHz and 40 at 94 GHz). This is referred to as the *swept-field* calculation in the original literature about the EPRLL program.[10,11] For MOMD calculations, it is necessary to repeat the swept-field calculation at each of the director tilt angles used in the calculation (n_{ort}).

Once the swept-field calculation is accomplished, the maximum projection of each basis vector on the set of $|u\rangle$ vectors is tabulated, normalized, and stored in a basis set file as a set of *significance* or *weighting factors* for each element of the basis vector. The vectors in the starting basis set may be selected into a "pruned" set by specifying a *pruning tolerance*. Only basis vectors with weighting factors larger than the pruning tolerance are retained in a pruned basis set.

It is possible to "over-prune" the basis (i.e., to specify too large a pruning tolerance) to the point it works only for a very narrow range of physical parameters. The symptoms of an insufficient basis set are often less apparent than in the case where the truncation parameters are too small. Although pruning tolerances of up to 0.03 have been used,[30] we recommend a more conservative value of 0.003 for general use. This tolerance represents a reasonable compromise between computational efficiency and flexibility. Even smaller tolerances may be required for the slowest motions at high ESR frequencies. It is advisable to check the calculation by reducing the pruning tolerance until the calculated line shape does not change significantly with the tolerance. This can be accomplished by starting with an oversized basis set, to avoid repeating an entire field-swept calculation for each relevant range of parameter values.

TABLE 6. Control Parameters Used in EPRLL Programs

Symbol	Name	Description
B_0	**b0**	Spectrometer field in gauss
	cgtol	Tolerance for conjugate gradient iterations
	range	Spectrum field range in gauss
ν	**freq**	Spectrometer frequency in GHz
ϕ	**phase**	Phase of spectrum in degrees: 0° = absorption, 90 = dispersion
	shiftr, shifti	Real and imaginary parts of diagonal shift term added to matrix in CG solution
	ideriv	Derivative mode (0 = absorption, 1 = 1st derivative)
$p^{\mathrm{I}}{}_{\mathrm{mx}}$	**ipnmx**	Maximum nuclear transition quantum number in basis set ($0 \leq$ ipnmx $\leq$ in2)
K_{mx}, K_{mn}	**kmx, kmn**	Maximum and minimum K quantum number in basis set (kmn $\leq 0 <$ kmx $<$ lemx)
L_{emx}, L_{omx}	**lemx, lomx**	Maximum even and odd L quantum number used in basis set ($0 <$ lomx $<$ lemx)
$m_\perp$, $m_\parallel$	**mprp, mpll**	Model flags for non-Brownian diffusion perpendicular and parallel to diffusion z (1=free, 2= jump diffusion)
M_{mx}, M_{mn}	**mmx, mmn**	Maximum and minimum M quantum number in basis set (mmn $\leq 0 <$ mmx $<$ lemx)
	ipdf	Diffusion model (0 = Brownian; 1 = non-Brownian, 2 = anisotropic viscosity)
n_{field}	**nfield**	Number of field positions in spectrum
n_{ort}	**nort**	Number of MOMD orientations (0 for no MOMD)
n_{step}	**nstep**	Maximum number of conjugate gradient steps allowed in tridiagonal matrix calculation

The control parameters used in the EPRLL programs are summarized and defined in Table 6.

4. NONLINEAR LEAST-SQUARES ANALYSIS

The physical parameters in the models described above are most usually obtained from experimental slow-motional ESR spectra using nonlinear least-squares (NLLS)

analysis, in which a subset of m parameters is iteratively refined to minimize the quantity

$$\chi^2 = \frac{1}{n-m}\sum_{i=1}^{n}\left(y_i - f(B_i,\mathbf{x})\right)^2 \tag{7}$$

where (B_i,y_i) are the experimental field and intensity values, f is the line shape function, and $\mathbf{x}$ is a vector of search parameters. Assuming that a global minimum in χ^2 is located at $\mathbf{x} = \mathbf{x}^*$ the parameter values in $\mathbf{x}^*$ are taken to be the "solution", that is, the values given by the experimental spectrum.

A wide variety of methods are available to accomplish the minimization described above.[31] In all but the simplest cases, programs designed to carry out NLLS using the SLE line shape calculation are computationally quite demanding, so it becomes important to reduce the number of iterations during the fitting procedure as much as possible, especially when fitting for many parameters. This can be achieved by using a suitable fitting algorithm, as well as by gaining an understanding of the behavior of the model itself and the correlations among the fitting parameters. We conclude by briefly discussing the two most common approaches, which include (*1*) variants of the basic Gauss–Newton method, including the Levenberg–Marquardt algorithm,[15] and (*2*) the Nelder–Mead, or "downhill simplex", search.[32,33]

The most widely distributed program for least-squares analysis is the NLSL program distributed by the Freed group at Cornell, which is based on the Levenberg–Marquardt method.[15] This method is designed to provide quadratic convergence from an arbitrary starting point to a minimum in χ^2. In principle, this should be significantly faster than downhill search methods such as the Nelder–Mead algorithm.[31] One potential drawback of Gauss–Newton methods is that they require estimation of the Hessian, or curvature, matrix, that is, an m by m matrix of second derivatives $H_{ij} = \partial^2(\chi^2)\ \ \partial x_i \partial x_j$. This matrix is typically estimated by calculating the first derivatives of χ^2 using the forward-difference approximation, which requires $m + 1$ line shape calculations per iteration. The rapid convergence of Gauss–Newton methods generally compensates for this computational burden, and they have the additional advantage that parameter uncertainties may be estimated from the curvature matrix.[15]

However, a more serious difficulty with such methods is that accurate derivatives require much closer convergence of the SLE calculation to the "true" spectrum. Basis sets and tolerance parameters that lead to a satisfactory spectrum can still produce unacceptable oscillations in the derivatives of that spectrum with respect to the calculation parameters, significantly slowing convergence of the minimization. Our own side-by-side comparison of the Levenberg–Marquardt and Nelder–Mead methods suggests that, although the downhill simplex algorithm requires more iterations to locate the minimum, the minimization is often accomplished with a comparable number of line shape calculations. Given that the Gauss–Newton method is more computationally demanding for each line shape calculation, the Nelder–Mead search may be a competitive alternative in many cases.

With the widespread use of commercially available computational software packages, it has become possible to adapt ESR line shape analysis to specific needs by

simply interfacing it line shape calculation to the appropriate software. Several groups currently use the LabView[34] program based on the EPRLL calculation that was originated by the Hubbell group at UCLA.[35] Recently, a version of the EPRLL program that is callable from a wide variety of computational packages, such as Matlab,[36] MathCad,[37] and Mathematica,[38] has been released (see the section *Appendix: Program Availability* below). This capability should greatly facilitate the adaptation of slow-motional line shape calculations to include new methods for fitting multicomponent spectra,[39,40] obtaining global fits to multifrequency spectra,[26] or carrying out global fits including other types of physical measurements.[41] Such flexibility promises to significantly enhance the information obtainable from ESR spectra of spin-labeled polymers in the future.

ACKNOWLEDGMENTS

K.A. Earle thanks the ACERT center at Cornell University for the use of its facilities during the preparation of this manuscript. ACERT is supported by National Institutes of Health NCRR grant RR016292. D.E. Budil gratefully acknowledges support from the Institute for Complex Scientific Software in the College of Computer Science at Northeastern University.

APPENDIX: PROGRAM AVAILABILITY

The calculations described in this chapter refer specifically to the EPRLL programs distributed by the Center for Advanced ESR Technology (ACERT). The ACERT website has a number of useful programs available for FTP downloading in the directory ftp.ccmr.cornell.edu/pub/freed. This directory can be accessed by anonymous FTP to ftp.ccmr.cornell.edu. Numerous research groups all over the world have availed themselves of these programs. The programs source codes are stored in uncompressed format and may be obtained by standard text (ASCII) ftp transfer. Tar files are provided for compressed data transfer and contain all files in the specific directories and subdirectories except the executables to save space. The available software packages relevant to this chapter include the following:

PC: Contains the original pc version of the CW spectrum simulation programs (Ref. 10).

PC.NEW: A new addition that contains a version of the EPRLL programs suitable for running on a pc with Windows 95. Only the source files that have been changed from the EPRLL directory are included, plus the executables. See the README file on that directory.

EPRLL: Contains the basic simulation program for CW spectrum calculation including the program EPRBL used to determine the truncated basis sets.

NLSL: Contains the Windows-compatible least squares version of the above CW program using Marquardt–Levenberg minimization. See the subdirectory EXAMPLES for fitting examples to test (Ref. 15).

MATLAB: Contains the EPRLL line shape calculation engine (a dynamic load library, or DLL file) that is callable from MATLAB for use in customized least-squares optimization.

NLSL.SRLS: Performs fitting for multi-frequency ESR spectra using the Slowly Relaxing Local Structure (SRLS) model (Ref. 26).

Free use and distribution of these programs is permitted with suitable reference to the original publication (see above) in any published work resulting from the use of these programs or programs derived from them. The programs may be copied and distributed, so long as: (1) due credit is given by retaining the comment lines at the beginning of each source file in all copies; and (2) all copies must be distributed free of charge.

Every effort has been made to ensure that these programs are correct and thoroughly tested. However, the programs are distributed "AS IS", and all warranties, whether expressed or implied, as to correctness or fitness for any specific purpose are specifically disclaimed. In no event shall the authors be liable for any direct, consequential or incidental damages arising from the use of these programs. The READ.ME files are provided in each of the above directories giving further information on their contents and usage. Please check the file CORRECTIONS in the directories for important information and code updates.

Another popular and widely available package that may be used to model and fit ESR spectra of nitroxides in the slow-motional regime is EasySpin (S. Stoll and A. Schweiger, "EasySpin, a comprehensive software package for spectral simulation and analysis in EPR," *J. Magn. Reson.*, **178**: 42–55, 2006, available at http://www.easyspin.ethz.ch/). The programs also model spectra in the fast-motion and rigid limits, and are based in the Matlab computational package, affording significant graphical capabilities and ease of use. Compared to the EPRLL programs described in this chapter, EasySpin has the additional capability to approximate the slow-motion spectrum of a radical with multiple nuclei; however, the present version does not include a local ordering potential.

REFERENCES

1. *Spin Labeling I. Theory and Application,* Berliner, L.J., Ed.; Vol. 1. New York: Academic Press, 1976.
2. *Biological Magnetic Resonance,* Berliner, L.J., Reuben, J., Eds.; New York: Plenum Press, 1989; Vol. 8, 444 pp.
3. Likhtenshtein, G.I. *Biophysical Labeling Methods in Molecular Biology*. Cambridge: Cambridge University Press, 1993.
4. Robinson, B.; Slutsky, L.; Auteri, F. *J. Chem. Phys* **1992**, *96*, 2609.
5. Hakansson, P.; Westlund, P.; Lindahl, E.; Edholm, O. *Phys. Chem. Chem. Phys.* **2001**, *3*, 5311.
6. Steinhoff, H.-J.; Hubbell, W.L. *Biophys. J.* **1996**, *71*, 2201.

7. Freed, J.H. In *Spin Labeling*, L.J. Berliner, Ed.; Academic Press: New York. 1976; p. 53.
8. Kubo, R.; Tomita, K. *J. Phys. Soc. (Jpn)* **1954**, *9*, 8.
9. Moro, G.; Freed, J.H. *J. Phys. Chem.* **1980**, *84*, 2837.
10. Schneider, D.J.; Freed, J.H. *Biol. Magn. Reson.* **1989**, *8*, 1.
11. Schneider, D.J.; Freed, J.H. *Adv. Chem. Phys.* **1989**, *73*, 387.
12. Moro, G.; Freed, J.H. *J. Chem. Phys.* **1981**, *74*, 3757.
13. Meirovitch, E.; Igner, D.; Igner, E.; Moro, G.; Freed, J.H. *J. Chem. Phys.* **1982**, *77*, 3915.
14. Lee, S.; Budil, D.E.; Freed, J.H. *J. Chem. Phys.* **1994**, *101*, 5529.
15. Budil, D.E.; Lee, S.; Saxena, S.; Freed, J.H. *J. Magn. Reson, Ser. A* **1996**, *120*, 155.
16. Ding, Z.; Gullà, A.F.; Budil, D.E. *J. Chem. Phys.* **2001**, *115*, 10685.
17. Brustolon, M.; Maniero, A.L.; Corvaja, C. *Mol. Phys.* **1984**, *51*, 1269.
18. Zare, R.N. *Angular Momentum: Understanding Spatial Aspects in Chemistry and Physics*; John Wiley & Sons, Inc., New York: 1988; 346 pp.
19. Marek, A.; Czernek, J.; Steinhart, M.; Labsky, J.; Stepanek, P.; Pilar, J. *J. Phys. Chem. B* **2004**, *108*, 9482.
20. Pilar, J.; Labsky, J.; Marek, A.; Budil, D.E.; Earle, K.A.; Freed, J.H. *Macromolecules* **2000**, *33*, 4438.
21. Liu, Z.; Ottaviani, M.F.; Abrams, L.; Lei, X.; Turro, N.J. *J. Phys. Chem. A* **2004**, *108*, 8040.
22. Ottaviani, M.F.; Lei, X.-G.; Liu, Z.; Turro, N.J. *J. Phys. Chem. B* **2001**, *105*, 7954.
23. Barnes, J.P.; Freed, J.H. *Biophys. J.* **1998**, *75*, 2532.
24. Polnaszek, C.F.; Bruno, G.V.; Freed, J.H. *J. Chem. Phys.* **1973**, *58*, 3185.
25. Meirovitch, E.; Nayeem, A.; Freed, J.H. *J. Phys. Chem.* **1984**, *88*, 3454.
26. Liang, Z.; Freed, J.H. *J. Phys. Chem. B*, **1999**, *103*, 6384.
27. Polimeno, A.; Freed, J.H. *J. Phys. Chem.* **1995**, *99*, 10995.
28. Sastry, V.S.S.; Polimeno, A.; Crepeau, R.H.; Freed, J.H. *J. Chem. Phys.* **1996**, *105*, 5753.
29. Sastry, V.S.S.; Polimeno, A.; Crepeau, R.H.; Freed, J.H. *J. Chem. Phys.* **1996**, *105*, 5773.
30. Vasavada, K.V.; Schneider, D.J.; Freed, J.H. *J. Chem. Phys.* **1987**, *86*, 647.
31. Press, W.H.; Teukolsky, S.A.; Vetterling, W.T.; Flannery, B.P. *Numerical Recipes in C: The Art of Scientific Computing*. New York: Cambridge University Press, 1992; 994 pp.
32. Duling, D.R. *J Magn Reson B* **1994**, *104*, 105.
33. Fajer, P.G. *Biophys. J.* **1994**, *66*, 2039.
34. Labview, National Instruments, Austin, TX.
35. Altenbach, C., personal communication.
36. Matlab, The Math Works, Inc., Natick, MA.
37. Mathcad, MathSoft Engineering and Education, Inc., Cambridge, MA.
38. Mathematica, Wolfram Research, Inc., Champaign, IL.
39. Baumann, B.A.;Liang, H.; Sale, K.; Hambly, B.D.; Fajer, P.J. *Biophys J*. **2004**, *86*, 3030.
40. Strancar, J.; Koklic, T.; Arsov, Z. *J Membr. Biol*, **2003**, *196*, 135.
41. Hustedt, E.J.; Cobb, C.E.; Beth, A.H.; Beechem, J.M. *Biophys J*. **1993**, *64*, 614.